Computational and Structural Biotechnology Journal 19 (2021) 5466–5478

COMPUTATIONAL AND STRUCTURAL BIOTECHNOLOGY JOURNAL

journal homepage: www.elsevier.com/locate/csbj

# Structural inspection and protein motions modelling of a fungal glycoside hydrolase family 18 chitinase by crystallography depicts a dynamic enzymatic mechanism

Elena Jiménez-Ortega [a], Peter Elias Kidibule [b], María Fernández-Lobato [b,*], Julia Sanz-Aparicio [a,*]

[a] Department of Crystallography and Structural Biology, Institute of Physical Chemistry Rocasolano, CSIC, 28006 Madrid, Spain
[b] Department of Molecular Biology, Centre of Molecular Biology Severo Ochoa, CSIC-UAM, 28049 Madrid, Spain

ARTICLE INFO

*Article history:*
Received 22 July 2021
Received in revised form 21 September 2021
Accepted 26 September 2021
Available online 2 October 2021

*Keywords:*
Chitinase
Crystal structure
Chitin oligosaccharide
Binding mode
Dynamic mechanism
Specificity

ABSTRACT

Chitinases degrade chitin into low molecular weight chitooligomers, which have a broad range of industrial, agricultural, and medical functions. Understanding the relationship between the diverse characteristics of chitinases and their functions is necessary for the improvement of functional enzymes that meet specific requirements. We report here a full crystallographic analysis of three complexes obtained from the chitinase Chit42 from *Trichoderma harzianum*, which represent different states along the enzymatic mechanism. The inactive double mutant D169A/E171A was submitted to soaking/crystallization experiments with hexa-N-acetyl-glucosamine (NAG6) or tetra-N-acetyl-glucosamine (NAG4), trapping the enzyme-substrate complex (Chit42-NAG6), the enzyme-products complex (Chit42-NAG4-NAG2) and a someway intermediate state. Structural comparison among the different complexes depicts the determinants defining the different subsites and revealed a previously unobserved dynamic on-off ligand binding process associated with a motion of its insertion domain, which might be accompanying the role or aromatics in processivity. An ensemble refinement performed to extract dynamic details from the diffraction data elucidates the implication of some highly flexible residues in the productive sliding of the substrate and the product release event. These positions were submitted to mutagenesis and the activity of the variants was investigated in the hydrolysis of NAG6, colloidal chitin and two chitosans with different polymerization and acetylation degree. All the changes affected the Chit42 hydrolytic activity therefore confirming the involvement of these positions in catalysis. Furthermore, we found the variants R295S and E316S improving the apparent catalytic efficiency of chitin and NAG6 and, together with E316A, enhancing the specific activity on chitosan. Therefore, our results provide novel insight into the molecular mechanisms underlying the hydrolysis of chitinous material by fungal chitinases, and suggest new targets to address engineering of these biotechnologically important enzymes.



## 1. Introduction

Chitin, one of the most widespread polysaccharides in nature, is a linear polymer of β1-4-linked N-acetyl glucosamine (NAG) units. This biopolymer is part of the exoskeleton of insects, crustacean shells, fungi cell-walls, microfilaria sheath of parasitic nematodes, and structural elements of some marine species [1]. The partial deacetylation of chitin results in the production of chitosan. Degradation of chitin and chitosan produces chitooligosaccharides (COS), which are endowed with biocompatibility, biodegradability, non-toxicity, and adsorption properties [2]. COS are being subject of increasing interest in terms of their pharmaceutical and medicinal applications owing to their activity as anti-oxidant, anti-inflammatory, anti-viral, anti-microbial, anti-tumoral, anti-hyperthensive or as prebiotics [3–5]. COS vary in degree of polymerization (DP), degree of deacetylation (DD), and pattern of acetylation (PA), and can be produced by chemical hydrolysis from chitin and chitosan, but the process is hard to control and generates undesirable and persistent by-products. Alternatively, the

*Abbreviations:* GH, glycosyl hydrolase; CID, chitinase insertion domain; COS, chitooligosaccharides: NAG, N-acethyl glucosamine; Chit42, chitinase from *Trichoderma harzianum*; SmChitA, chitinase A from *Serratia marcescens*; SpChitD, chitinase D fron *Serratia proteamaculans*.

* Corresponding authors.
*E-mail addresses:* mfernandez@cbm.csic.es (M. Fernández-Lobato), xjulia@iqfr.csic.es (J. Sanz-Aparicio).

https://doi.org/10.1016/j.csbj.2021.09.027
2001-0370/

enzymatic hydrolysis of chitin and chitosan has revealed as the most effectively product-controlled and environmental-friendly method [6]. Therefore, much effort is required to fully depict the mode of action and the substrate specificity of chitinolytic enzymes, with the goal of applying protein engineering to develop efficient enzymes for biotechnological applications.

Glycosyl hydrolase (GH) families 18, 19 and 20 include chitinolytic enzymes catalyzing the degradation of chitin polymers. GH18 chitinases represent an ancient type of enzymes found in all kingdoms of life, sharing a catalytic TIM-barrel domain and showing a substrate-assisted catalytic mechanism where a conserved glutamate residue (included in the DXDXE catalytic motif) protons the glycosidic bond to be hydrolyzed (forming an oxazolinium ion intermediate), and the oxygen of the N-acetyl group of NAG in the subsite −1 sugar acts as nucleophile [7,8]. Evidences from kinetic studies, crystal structure analysis and molecular dynamics simulations depicted crucial features as the role of the catalytic aspartates, the stabilization of the oxazolinium intermediate by the enzyme, or the distortion of the stereochemistry of substrates leading to glycosidic bond cleavage (for an updated review see [9] and references therein).

Chitinases are classified into *endo*- and *exo*-acting enzymes according to their cleavage type, with the first catalyzing internal hydrolysis of chitin chains at random positions while the second degrades the ends of the polymer chain, either the reducing or non-reducing end, generating primarily chitobiose (NAG2) [10]. In addition, many chitinases present processive ability mostly producing disaccharides with relatively few odd-numbered saccharides [11,12] which is considered beneficial for the hydrolysis of crystalline chitin while it may be a rate-limiting process with soluble substrates [13]. In general, *exo*-acting chitinases are processive enzyme while *endo*-acting chitinases are non-processive. The structural basis of processivity has been uncovered in the *Serratia marcesces* chinilotityc system, which includes two multimodule *exo*-acting processive (SmChiA and SmChiB) and one *endo*-acting (SmChiC) [14]. Processivity has been mostly attributed to deep substrate-binding cleft topology and to the presence of aromatics in the catalytic groove, the latter being assessed by mutagenesis studies [10,13,15], However, new evidences point to a putative role in processivity of the polar residues lining the binding cleft [16] revealing that further work is needed to have a clear picture of the sophisticated molecular basis of processivity, which will return in a better understanding of the degradation of recalcitrant polymers.

Hydrolysis is the most common process performed by these enzymes and occurs when a water molecule attacks the oxazolinium ion intermediate with the subsequent biopolymer breakdown. In addition, some chitinases also show transferase activity that arises when these retaining glycosidases trigger the transfer of a glyosidic residue, instead of a water molecule, from a donor to an acceptor substrate yielding a longer COS chain. Although this reaction is secondary to the hydrolytic activity, the balance can be kinetically controlled and has been proved to be modulated by mutagenesis of key residues at the catalytic site, and also by removal of some aromatics at the active site groove of chitinases from *Serratia* [17]. Thus, mutations leading to decreased rate of hydrolysis and enhanced sugar acceptor-binding access may result in an increased level of TG products [18]. Therefore, a full understanding of the catalytic mechanism and depiction of subsites affinities is required to fully exploit the synthetic use of chitinases. However, despite much work has been reported in the last years on bacterial chitinases, mostly from *Serratia*, only mutagenesis experiments of the three conserved catalytic residues has been explored through the glycosynthase strategy in fungal chitinases [19]. Therefore, additional work is required to take full advantage of this important group of enzymes. Moreover, an interesting issue is the fact that partially deacetylated chitooligosaccharides are hydrolyzed slower than fully acetylated, which is valuable to generate transglycosylases [12]. Consequently, chitosan is an interesting target to explore as source of COS.

This work is focused on Chit42 from the fungus *Trichoderma harzianum* that works through an *exo*-, processive mechanism. Previously, we reported the structure of Chit42 wild type and evaluated its hydrolytic activity in presence of substrates with different polymerization and acetylation degree. Consequently, high variety of COS products, specially NAG2 and NAG3, were identified [20]. Recently, we attempted the immobilization of this enzyme on different supports and the effectiveness of the immobilized biocatalyst in the production of COS by the bioconversion of colloidal chitin and chitosan was evaluated [21]. In the present study, different protein variants of Chit42 were heterologously expressed in *Pichia pastoris* and three different complexes were obtained and analyzed using X-ray crystallography. The different binding sites were depicted and the protein motion was modelled by combining diffraction data with molecular dynamics simulation. The results uncover the molecular determinants behind the slide of the substrate through the catalytic tunnel and the product release mechanism. The structural analysis has been key in order to select the suitable mutations to modify the Chit42 hydrolytic activity. The effect of proposed Chit42 mutations on several substrates with different polymerization and acetylation was evaluated.

## 2. Materials and methods

### 2.1. Materials

Chitin (from shrimp shells, coarse flakes; DD $\leq$ 8), glucosamine and chitosan CHIT50 (MW 50–190 kDa; DD 77%) were from Sigma Aldrich (St. Louis, MO, USA). N,N',N'',N'''-acetyl chitotetraose (NAG4) and N,N',N'',N''',N'''', N'''''-acetyl chitohexaose (NAG6; 1237 Da) were from Carbosynth Ltd (Berkshire, UK). Chitosan solutions and colloidal chitin preparation were obtained as previously [20] but for the last some modifications were made. Briefly: 50 g of chitin flakes were suspended in HCl (10 M) for 16 h followed by precipitation using cold water (5 L), and after 24 h the suspension was washed using water until neutral pH was reached. Chitosan CHIT100 (MW 100–300 kDa; DD > 90%) was from Acros Organics (Thermo Fischer Scientific Inc., Waltham, MA). Yeast Nitrogen Base w/o amino acids (YNB) was from Difco (BD, Sparks, MD, USA). All reagents were of the highest purity grade.

### 2.2. Strains, expression media, plasmids, and site directed-mutagenesis

*Pichia pastoris* GS115 (*his4*-) (Invitrogen, Carlsbad, CA, USA) was used as expression host, and was cultured at 30 °C and 250 rpm shaking in YEPD (1% yeast extract, 1% peptone, 2% glucose; all w/v). The yeast transformants were selected on MD (1.3% YNB, 4 mg $mL^{-1}$ biotin, and 2% glucose). Expression of the proteins in *P. pastoris* was analyzed on BMM after growing in BMG (both MD including 100 mM potassium phosphate pH 6.0 and 0.5% methanol or 1% glycerol, respectively). Microbial growth was monitored spectrophotometrically at a wavelength of 600 nm ($OD_{600}$), and protein concentration was determined using NanoDrop at 280 nm. At the maximum time of induction, cells were removed by centrifugation (6000xg for 15 min) and extracellular protein fraction was concentrated (if required) using 30-kDa MWCO PES membranes and a Vivaflow 50 system (Sartorius, Gottingen, Germany). The *Escherichia coli* DH5α strain was used as host for DNA manipulations using the standard techniques.

The gene *chit42* from *Trichoderma harzianum* CECT2413 comprises an open reading frame of 1272-bp (GenBank accession no.

S78423.1) including the stop triplet and coding for a protein of 423 amino acids (P48827). In this work, plasmid CHIT42-pIB4, which contained the gene *chit42* fused to the 267-bp fragment of the *Saccharomyces cerevisiae* MFα secretion signal sequence, was used as template to obtain all the protein variants generated in this study [20]. In addition, expression of Chit42 was under the control of *AOX*1p, which means that protein production can be strongly induced by methanol. Site-directed mutagenesis was carried out using a restriction enzyme free strategy with Phusion High-fidelity DNA polymerase (NEB, Ipswich, UK) and a pair of specific primers (Table S1, in supplementary material), including mutations responsible for substitutions Y172E/F, F240N, F245N, R294A/S/T, E316N/S, W378A, E171A, D169N/E171A and D169A/E171A as referred previously [22]. The PCR conditions were: (i) 98 °C for 30 s; (ii) 25 cycles of 98 °C for 10 s, 55 °C for 30 s and 72 °C for 144 s; (iii) final extension at 72 °C for 600 s. The PCR reactions were treated with *Dpn*I to eliminate the parental plasmid and transformed into *E. coli*. Mutations (and integrity of the constructions) were verified by DNA sequencing using primers: AOX1: 5′-GACTGGTTCCAATTGACAAGC-3′ and AOX2: 5′-CCTA CAGTCTTACGGTAAACG-3′, both from Sigma Aldrich (St. Louis, MO). Constructions including the desired mutation were linearized with *Stu*I (into *His4* of the pIB4 derivatives) transformed in *P. pastoris* by electroporation, and confirmed by PCR as referred [20]

### 2.3. Hydrolytic activity

The chitinase activity of the different Chit42 variants was determined using the 3,5-dinitrosalicylic acid (DNS) assay adapted to a 96-well microplate as explained in previous study [20]. Briefly, the reactions were performed in 1.5 mL Eppendorf tubes by the addition of 100 μL of the enzymatic solution (undiluted) to 400 μL of 1% (w/v) colloidal chitin and other substrates (all substrates were at pH 5.0). Tubes were incubated at 900 rpm in a Thermo Shaker TS-100 (Boeco, Hamburg, Germany) for 1 at 35 °C. To stop the reactions, the tubes were boiled for 10 min and one volume of 0.2 M NaOH added to precipitate the non-hydrolyzed polysaccharides. A calibration curve of NAG (0–3 mg $mL^{-1}$) was used. One unit of activity (U) corresponded to the release of one μmol of reducing sugars per minute. Kinetic constants were determined using 0.1–15 mg $mL^{-1}$ of colloidal chitin as substrate. For NAG6 25–1500 μM was used. The plotting and analysis of the curves was carried out using GraphPad Prism software (version 6.0), and the kinetic parameters were calculated fitting the initial rate values to the Michaelis-Menten equation. Standard errors were obtained by fitting the normalized equation as $v = (k_{cat}/K_m)[S]/(1 + [S]/K_m)$.

### 2.4. Crystallization, X-ray structure determination of complexes and molecular dynamic refinement of Chit42.

Reported crystallization conditions of Chit42 included 0.2 M zinc acetate [20], which was shown to block the catalytic site impeding binding of substrates to the different inactivated mutants tested. However, the presence of this molecule was essential for crystal growing and additional screening for new conditions was unsuccessful. Then, the native reported conditions were reproduced including a treatment of the protein or the crystals with EDTA, to modulate the free $Zn^{2+}$ levels.

The complexes of the Chit42-NAG6 and NAG4/NAG2 were obtained by the soaking technique. Preformed crystals of D169A/E171A double mutant (grown by mixing 7.3 mg $mL^{-1}$, 50 mM Tris HCl, pH 7.0 protein solution with 18–19% polyethylene glycol (PEG) 3000, 0.1 M zinc acetate, 0.1 M zinc chloride and 0.1 M imidazole pH 8.0, in a 1:1 ratio) were transferred to a soaking solution supplemented with 30 mM NAG6 or NAG4 and 2 mM EDTA for 30 min.

Cocrystallization technique was also tried to obtain the D169A/E171A double mutant complexed with NAG4. The protein (7.3 mg $mL^{-1}$ in 50 mM Tris HCl, pH 7.0), was pre-incubated at 4 °C with 2 mM EDTA for 2 h and, then, with 20 mM NAG4 for 4 h. Crystals were grown by mixing the protein solution with the precipitant solution (15% polyethylene glycol (PEG) 3000, 0.2 M zinc acetate, 3% 2-methyl-2,4-pentanediol (MPD) and 0.1 M imidazole pH 8.0) in a 1:1 drop ratio.

For data collection, crystals were transferred to cryoprotectant solutions consisting of mother liquor plus 20% PEG400 and 2 mM EDTA, being flash-cooled in liquid nitrogen. Furthermore, in the case of NAG4 co-crystallized complex, these solutions were also supplemented with 4 mM substrate. Diffraction data were collected using synchrotron radiation on the XALOC beamline at ALBA (Cerdanyola del Vallés, Spain). Diffraction images were processed with XDS [23] and merged using AIMLESS [24] from the CCP4 package [25]. The crystals were indexed in the $P4_12_12$ space group, with one molecule in the a.u. and 50% solvent content within the unit cell. Final data collection statistics are given in Table S2 (supplementary material). The X-ray structure of the complexes were solved by using the coordinates of native Chit42 (PDB code 6EPB). Final refinement, using Refmac [26] from CCP4 Program suite, led to final R factor given in Table S2, using TLS refinement in the final step of the refinement in the NAG6 complex. Model-building was performed with COOT [27]. To extract dynamical details from the X-ray data, the coordinates of native Chit42 were first re-refined using PHENIX [28], and then were used as input models for a time-averaged molecular dynamics refinement as implemented in the Phenix.ensemble-refinement routine, which was performed as described previously [29]. The figures were generated with PyMOL [30] and the atomic coordinates have been deposited in RCSB Protein Data Bank under the accession codes 6YLJ for the NAG6 complex, 6YN4 for the NAG4/NAG2 complex obtained by cocrystallization technique, and 7AQK for the NAG4 complex obtained by soaking.

## 3. Results and discussion

### 3.1. Structural traits of the complexes give insights into the Chit42 machinery

The reported three-dimensional structure of Chit42 showed the general structural features of the GH18 chitinases, with the catalytic residues Asp167, Asp169 and Glu171 within the characteristic $(\alpha/\beta)_8$ TIM-barrel topology [20]. In this work, different inactivated mutants of Chit42 were produced (E171A, D169N/E171A and D169A/E171A), being subsequently tried in crystallization experiments to capture the substrates in the active site. Only the double change to alanine in the D169A/E171A variant eliminated any residual hydrolytic activity, allowing us to obtain complexes of Chit42 with NAG6 and NAG4. The complex Chit42-NAG6 was obtained by the soaking technique and was solved to 1.75 Å resolution, the electron density maps showing this oligosaccharide occupying subsites −4 to +2 (Fig. 1**A and B**) thus in a substrate binding mode (subsites at the non-reducing/reducing end of the substrate are given negative/positive numbers, the hydrolysis occurring between subsites − 1 and +1).

However, different results were obtained with NAG4 depending on the technique used. A first Chit42-NAG4 complex was obtained by cocrystallization of the enzyme with NAG4, and was solved at 1.82 Å resolution. The electron density showed a molecule of NAG4 spanning subsites −4 to −1, and a NAG2 moiety at subsites +1, +2 that is supposed to mimic putative products position

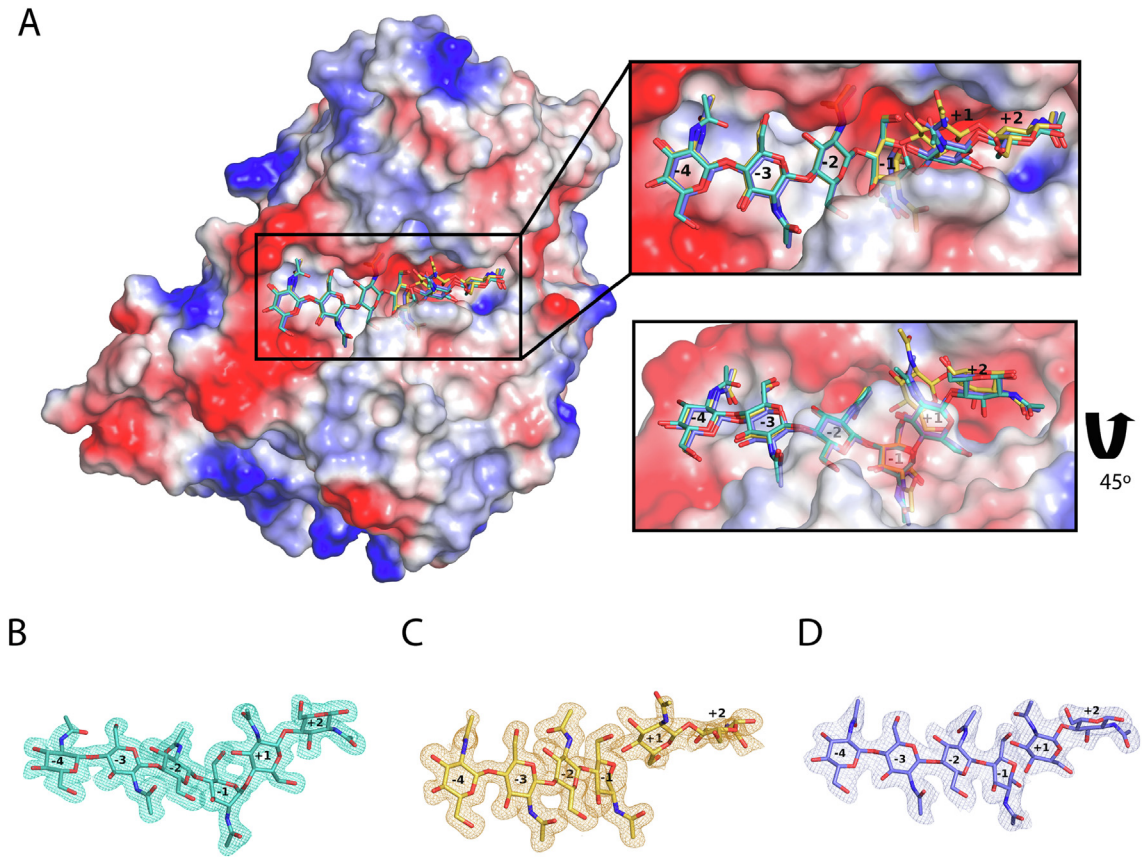


**Fig. 1. Chit42 crystal complexes**. A) Structural superposition of the Chit42 double mutant D169A/E171A complexed with NAG6 (teal) and NAG4/NAG2 (gold, cocrys; slate, soaking). Final 2Fo-Fc electron density map of the complexes with NAG6 (B), NAG4/NAG2 cocrys (C) and NAG4/NAG2 soaking (D), countoured at 1.0, 0.9 and 0.9 σ, respectively.

(Fig. 1**A and 1C**). On the other hand, soaking of the D169A/E171A mutant crystals into NAG4 led to X-ray data to 2.32 Å resolution revealing a slightly different complex. Thus, a NAG4 is spanning subsites −4 to −1, similarly to the complex obtained by cocrystallization described above, but a NAG2 molecule occupies subsites +1 to +2 in a different position (Fig. 1**A**). This state is supposed to represent the situation after the bond breakage but before the aglycon product migrates to the position observed in the NAG4 co-crystallized complex. The presence of a putative contaminant NAG6 can be discarded, as the clear electron density depicts the conformation of the two NAG units occupying subsites −1 and +1, and the absence of a covalent link **(**Fig. 1**D)**. The relevance of this complex structure in the mechanism and the binding affinity of the different subsites is discussed later. Experimental details and structure determination procedures are given in the Materials and Methods section and in Table S2.

The crystal structure of Chit42, previously reported by us, showed a $(\alpha/\beta)_8$ TIM-barrel as catalytic domain with an additional chitinase insertion domain (CID) (Fig. 2**A**). The TIM-barrel arrangement is composed of eight parallel ß- strands, which form the core, followed by eight α-helices, although α1-helix is missing. The active site is shaped by loops connecting the C-terminus of the β-strands to the α-helices, the connection of ß2 to α2 containing two extra antiparallel β-strands labeled as ß2a and ß2b. Additionally, the TIM-barrel presents a 60-residues insertion after β7, which corresponds to the CID-domain, contributing to make a shallow groove-like active site at its +1, +2 subsites. It is composed of a five ß-stranded β-sheet, comprising residues Tyr293 to Asp354. An analysis of the atomic B factor parameters (Fig. 2**B)** reveals that two regions present an obvious high chain mobility, i.e. the loop Asp84-Gly107 (linking ß2b to α2) and, specially, the complete CID domain. It is remarkable that the two complexes captured by soaking keep a similar B factor picture than the free enzyme, while the NAG4/NAG2 complex obtained by cocrystallization shows a CID domain that is somehow stabilized (Fig. 2**C)**. This means that oligosaccharide binding results in a more fixed domain, but this is observable only in the cocrystals that grow from the preformed, equilibrated complex.

Interestingly, structural comparison among the different complexes reveals a swing of the CID domain in the Chit42-NAG6 complex, which we associate to substrate binding/product release events (Fig. 2**D**). According to this, the CID domain approaches towards the catalytic domain upon NAG6 entrance, making a tighter interaction with the substrate, and retracts to the enzyme free-state withdrawing the products, a state represented by the Chit42-NAG4/NAG2 cocrystallization complex. This last state is also observed in the CID domain of the Chit42-NAG4/NAG2 soaked complex, although the atomic interactions depict a somehow intermediate situation. To our knowledge, this high CID flexibility has not been reported in other fungal or bacterial homologues, and we cannot exclude that it might be a trait of Chit42 rather than a general issue. Although the definitive role of the CID has not been completely understood, studies on homologous proteins demonstrated that this additional domain contributes to the binding affinity, facilitating the orientation and strong association with long substrates [31]. Our results suggest that it may also play a

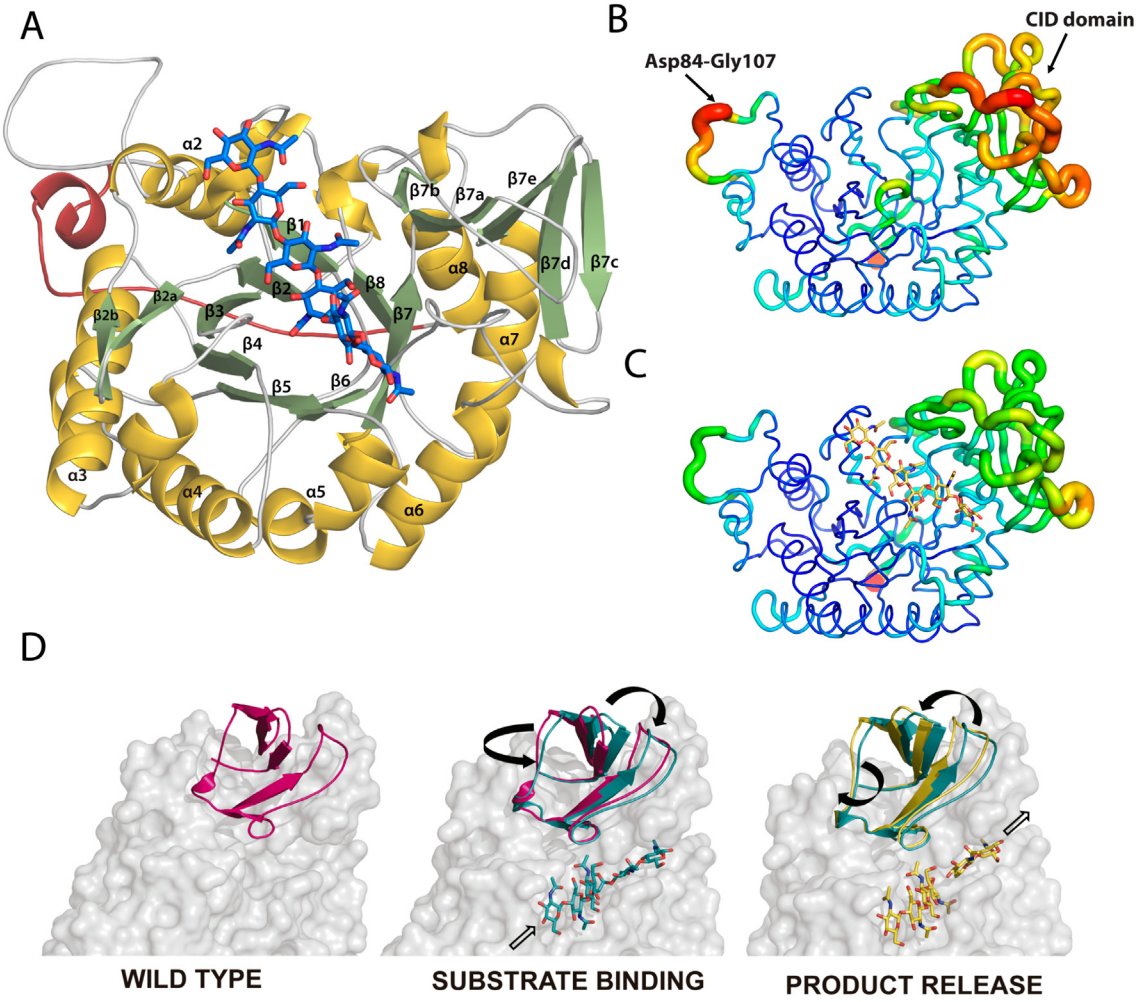


**Fig. 2. Chit42 structural features**. A) The general folding follows the $(\alpha/\beta)_8$ barrel topology with an additional CID domain, and a C-terminal extension that is colored in prune. B) a 90° rotation of A) showing chain flexibility, represented by the distribution of atomic B values along the chain in the unliganded enzyme, and C) in the Chit42-NAG4 complex obtained by cocrystallization. The two regions having highest mobility in the free enzyme (red color) are labelled. **D)** The swing at the CID domain observed in the complexes is ascribed to substrate binding/product release events. (For interpretation of the references to color in this figure legend, the reader is referred to the web version of this article.)

dynamic role in the reaction pathway facilitating the entrance of the substrates and/or the products release, by means of a molecular mechanism explained below.

A last interesting feature of the Chit42 folding is an insertion of 20 residues at its C-terminus, which makes and extended loop packed at the opposite face of the active site that ends in a short helix close to α2 (Fig. 2**A**). This structural feature is shared with the fungal enzymes but is absent in human and bacterial homologues (**Fig. S1,** supplementary material).

### 3.2. Comparison with other chitinases

The primary structure analysis determined that Chit42 showed 60–50% sequence identity with fungal chitinases (Crchi1 from *Clonostachys roseau*, PDB code 3G6L, [32]; AfChiB1 from *Aspergillus fumigatus*, PDB code 1W9P, [33]; CiX1 from *Coccidioides immitis,* PDB code 1D2K, [34], all of them having a very conserved fold with RMSD between 0.6 and 1.0 Å after superimposition to Chit42. Other homologues are bacterial and human chitinases, showing 30% sequence identity (considering the catalytic plus the CID domain), as ChiA74 from *Bacillus thuringiensis* (PDB code 6BT9 [35], RMSD 2.0 Å), ChiA from *Serratia marcescens (*PDB code 1NH6 [36], RMSD 1.7 Å), and human chitotriosidase (HuChtr from *Homo sapiens*, PDB code 1GUV) [37], RMSD 1.6 Å). These enzymes present some differences mostly, but not only, at their CID domains (**Fig. S1** in supplementary material).

As said before, the chitinolytic machinery expressed by *Serratia* has been largely studied as a model reference [12,14]. SmChiA and SmChiB are processive *exo*-acting chitinases moving into opposite directions, while SmChiC is a non-processive endochitinase that is supposed to primarily act on amorphous regions in the substrate. *Serratia proteamaculans* ChiD (SpChiD), a fourth chitinase hydrolyzing chitin and chitooliosaccharides, has been reported having an additional high degree of transglycosylation and chitobiase activity, therefore with an intriguing role on chitin degradation [38,39]. While SmChiC and SpChiD have only catalytic domain, SmChiA and SmChiB present additional carbohydrate-binding modules attached to their N-/ C-terminal sequences, respectively, which reflects their different reducing/non-reducing hydrolytic specificity. SmChiA, SmChiB and SpChiD belong to the GH18 bacterial subgoup including a CID insertion domain, while SmChiC is homologous to the plant-type GH18 enzymes. Chit42 presents reducing-end hydrolytic activity and, therefore, its catalytic domain resembles more that of SmChiA. The structural alignment of Chi42 to the three bacterial-type enzymes from *Serratia* is given in supplementary **Fig. S2**.

SmChiA has a fibronectin type III domain (FnIII) located at its N-terminal position putatively involved in binding the polymer. Interestingly, the bacterial FnIII domain is linked to β1-strand by an extended loop that is arranged similarly to the C-terminal extension of Chit42 (Fig. 3**A**), both being packed close to α2. Apparently, the C-terminal extension of Chit42 provides the same structural support than the bacterial FnIII domain to the long loop preceding α2 that delineates the distal subsites for binding chitin at the negative part of the active site (loop Asp84-Gly107 at ß2b-α2 in Chit42), which is the substrate binding site of the two enzymes according to the common reducing-end specificity. However, a significant difference between Chit42 and SmChiA is the longer loop linking β2 to α2 in the bacterial enzyme, which makes a larger structure protruding over the active site and making a narrower channel at its *minus* subsites. (Fig. 3**B**). Therefore, common molecular mechanisms may be behind the reducing/non-reducing hydrolytic mode of action, while significant structural determinants particular to each enzyme must be responsible for the different substrate specificity.

**Fig. S3** shows the structural comparison of Chit42 with SmChiB [8] and SpChiD [38], respectively. As it is observed, major differences between Chit42 and SmChiB are observed at the distal parts of the active site groove, with long insertions at its β1- β2 loop and the C-terminal attached CBD, which is consistent with its opposite hydrolytic affinity as compared to Chit42. In addition, the longer β7a-β7b loop of the CID domain makes a closer active site pocket. A similar long β7a-β7b loop is seen in the SpChiD CID domain and, in addition, very short β7a and β7b β-strands make a distorted CID domain, which might be related to this enzyme being non-processive. Moreover, large differences are also observed at loops β1-β2, β2-α2 and β4-α4. In fact, the high transglycosilation activity of SpChiD has been attributed to the loop β1-β2 that is folded close to the active site and is retracted upon substrate binding [39]. The implication of these structural differences in activity of the different enzymes will be discussed later.

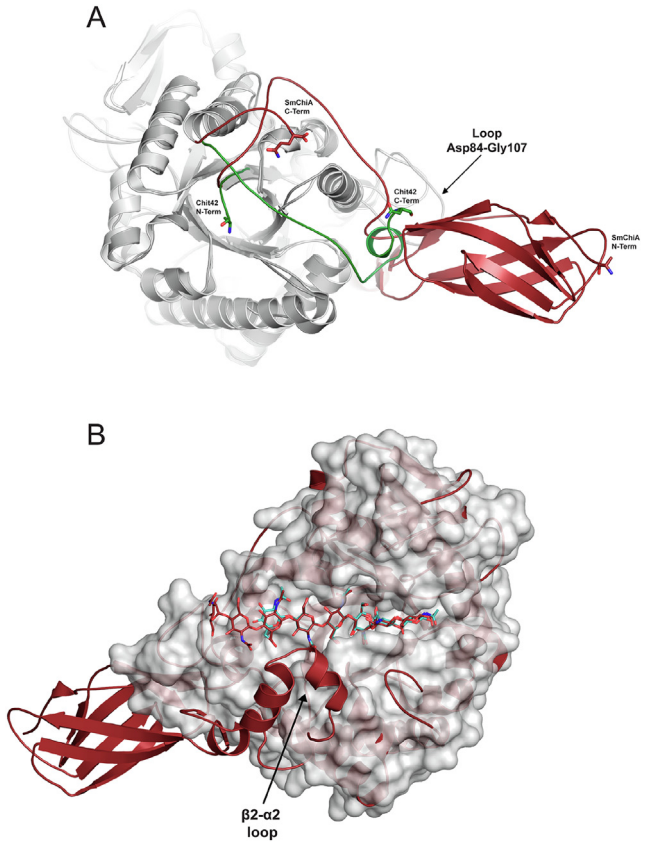


**Fig. 3. Chit42 vs SmChiA**. A) Superimposition of the SmChiA-NAG8 complex, (PDB code 1EIB) onto the Chit42-NAG6 complex in cartoon representation, highlighting the insertions at the SmChiA N-term (prune) and the Chit42 C-term (green). B) a 180° rotation showing the different contour of the active sites, with Chit42 represented as surface and NAG8 (prune), NAG6 (cyan) in sticks. (For interpretation of the references to color in this figure legend, the reader is referred to the web version of this article.)

### 3.3. Chit42 presents an extended active site

The structure of the Chit42 inactivated mutant complexed with NAG6 shows that the substrate binding site is a long, deep cleft with estimated dimensions of 30 Å (long) × 13 Å (deep) (Fig. 1**A**). The catalytic site conserves the DXDXE motif located at the end of β4-sheet **(Fig. S1)**, Glu171 being the proton donor catalyst and Asp169 stabilizing the oxazolinium intermediate. Our previous studies on unliganded Chit42 revealed a $Zn^{2+}$ ion coordinated to the catalytic Glu171 and to an acetate molecule from the crystallization solution, which apparently precluded the access of the substrates to the catalytic site. Therefore, different strategies were tested and the use of an EDTA complex agent was key to obtain the complexes**.** Some ions have been described to be bound in other Chit42 homologues [40]. For instance, $Zn^{2+}$ has been described to be strong inhibitor of *Bacillus cereus* chitinase [41] by interacting with critical residues and restricting hydrolysis capability. Similarly, the inhibitory effect by $Zn^{2+}$ observed in Chit42 (not shown) can be explained in terms of the $Zn^{2+}$ ion coordinating the catalytic Glu171 found in the native crystals.

As seen in Fig. 4**A**, Chit42 has at least six binding subsites allocating NAG6, from −4 to +2. The active site presents several conserved aromatic residues that would bind the substrate, allowing substrate translocation and processivity. Moreover, they seem also important structural element for *endo*-acting chitinases on soluble substrates [42]. Residues Trp98, Tyr86, Tyr50, and Trp47 are located on the extended surface at the entrance to the catalytic cleft in Chit42 (the "*minus* part"), and might guide the substrate towards the active site. In particular, Tyr86 and Trp98 show different conformation in the complexes and are located in the highly flexible loop linking ß2b to α2 described above (Fig. 2**B**), which suggests they might have an important role in processivity of long substrates. Furthermore, the sequence SXGGW has been described to be crucial for the processive activity in SmChiA [43]. This corresponds to residues 127 to 131 in Chit42, which includes Trp131. A Trp defining subsite +1 is common to bacterial and fungal-type chitinases, which also present a second aromatic at subsite +2, being a Trp in most fungal homologues but a Phe (Phe245) in Chit42, in common with SmChiA. This difference in the stacking surface interaction may be essential for specific ligand binding [33].

Thus, the presence of Tyr50 and Tyr86 at the entrance to the active site suggests that additional binding subsites are not discarded at this non-reducing end of the channel, as they seem in suitable position to interact with longer chitooligosacharides. Moreover, Trp98 could extend the platform for additional NAG units positioning. Fig. 4**B** shows a superimposition of Chit42-NAG6 onto the homologous human hcgp-39 glycoprotein, presenting NAG3 bound at subsites equivalent to −7 to −5 [44], which illustrates putative additional binding sites at this non-reducing end. Thus, Tyr50 may orient a potential NAG bound at subsite −5, similarly to the role played by Tyr34 in hcgp-39. The sugar could be further stabilized by a water-mediated hydrogen bond of its O6 to the Asp51 carboxylate (unique to Chit42) and, also, from the CO acetamide to Asp84. In fact, this Asp84 is linking an acetate moiety bound in our complex in a position close to the NAG acetamide reinforcing the existence of a well-defined subsite −5 in Chit42.

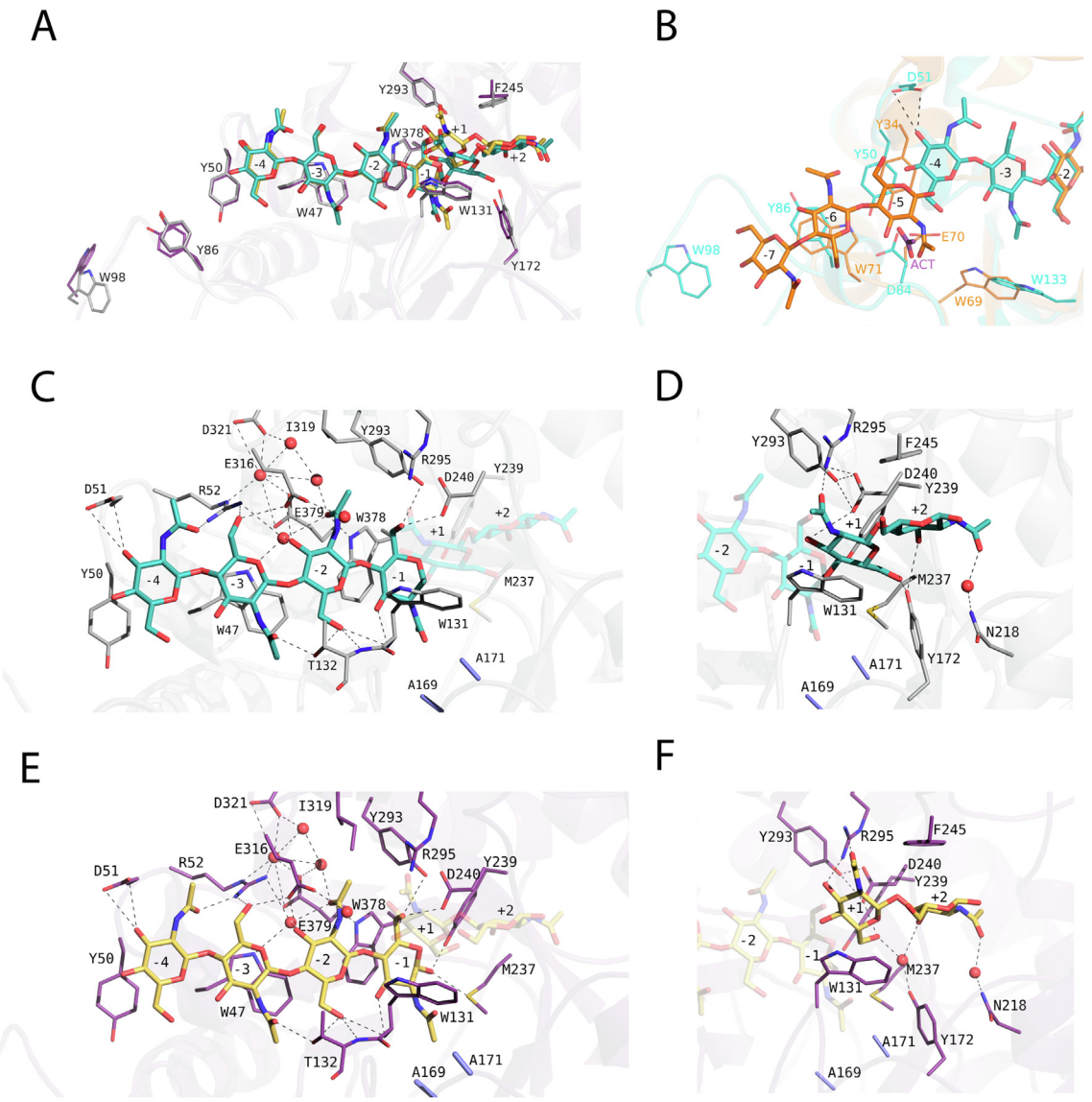


**Fig. 4. Substrate/product recognition pattern and binding mode.** A) Structural details of aromatic-mediated carbohydrate recognition in D169/E171 Chit42 at the catalytic cleft. The complexes with NAG6 and NAG4 are superimposed and shown in cyan and yellow, respectively. The residues, which are represented in gray (NAG6 complex) and purple (NAG4/NAG2 cocrystallization complex), would be crucial for the processive activity. B) Putative additional binding subsites in Chit42 (cyan) revealed by structural comparison with hcgp-39 chitin coordinates (orange) presenting NAG3 at subsite −5 to −7 (PDB code 1HJV). Relevant residues are shown. C) and D) Atomic interactions of NAG6 at the Chit42 active site, at the non-reducing and reducing-end, respectively; polar links represented as dashed lines. E) and F) Interactions in the complex with NAG4/NAG2 (cocrystallization) at the non-reducing and the reducing-end, respectively. (For interpretation of the references to color in this figure legend, the reader is referred to the web version of this article.)

A further NAG unit would be oriented at a putative subsite −6 by stacking to Tyr86 similarly to the role of Trp71 in the hcgp-39 complex. Addition of successive NAG rings at the non-reducing end would most likely fit the oligomer chain stacked to Trp98. Interestingly, SmChiA and the fungal Chit42 homologues present two aromatics at these positions. Consequently, although possibly not contributing to a substantial increase in binding affinity, they may be essential in orienting the polymer or long substrates, and for correct sliding of the chitin chain contributing to processivity.

In addition to this aromatic patch, the different complexes shown here reveal that some flexible residues might also contribute to the processive mechanism. An example is Glu316, placed between subsites −3 and −2, which presents different conformations in the complexes, suggesting a flexibility that could cooperate with the aromatic residues to slide the substrate along the tunnel. This issue is commented below.

### *3.4. Structural determinants of the binding subsites at the non-reducing-end*

To have a detailed picture of the different subsites, we have compared the Chit42-NAG6 and the Chit42-NAG4/NAG2 (cocrystallization) complexes, as representatives of the substrate/products bound at the Chit42 active site. At subsite −4, Arg52 participates in the CO positioning of the bound NAG (Fig. 4**C and 4E**). Slightly different N-acetyl positions are observed in the two complexes and, therefore, changes in this arginine could be translated into changes in the CO orientation. Moreover, this residue also interacts with O6 from the NAG in the subsite −3. Therefore, Arg52 might be a good candidate to promote the appropriate access of the ligand into the active site. In addition, Chit42 presents a bifurcated hydrogen bond between Asp51 carboxylate and the O3 oxygen. This aspartate is unique to Chit42, as the fungal homologues and also SmChiA and

human chitotriosidase present a glycine instead. Therefore, binding affinity of the NAG unit at this subsite seems stronger in Chit42, maybe explaining the preferred location of NAG4 at −4 to −1 subsites observed by cocrystallization, when a substrate binding mode at −2 to +2 could have been expected.

The NAG unit located at subsite −3 is oriented by hydrophobic interaction to Trp47, with many other polar interactions mediated by hydrogen bonds. Besides the link of O6 to Arg52 described above, Glu316 is hydrogen bonded to the O6 of NAG at subsite −3, and to O3 of the sugar at subsite −2; therefore, the carboxylate side-chain could act as a "clamp" between subsites −3 and −2. Furthermore, and showing a shift from the wild type structure, Thr132 approaches to the substrate forming a hydrogen bond with the CO group of the NAG in the complexes. Interestingly, these atomic interactions are fully conserved in SmChiA, despite the fact that largest differences in the shape of the Chit42 active site are observed in subsites −4 and −3 (Fig. 3**B**). Thus, it seems that the long insertion presented at the β2-α2 loop in the bacterial chitinase do not contribute with direct links to the extended NAG chain, although it may have some role in binding natural chitin.

The NAG unit bound at subsite −2 is tightly fixed by hydrogen bonds at all its oxygen atoms. First, O3 is linked to the Glu316 side-chain, as commented above, while O6 is linked to the Trp131 and Thr132 –NH– main-chain, and also to the Thr132 side-chain. Additionally, a direct hydrogen bond links the CO to the Trp378 side-chain, and a water-mediated link is made from Glu316 to the NH-acetyl. Furthermore, there is a conserved net of waters molecules near the CO connecting O3 and CO to Trp47 side-chain and to Arg52 and other distal polar residues, as Glu379 and Asp321. Finally, hydrophobic interactions of I319 can orient the NAG CH3 moiety. This strong binding is conserved in the SmChiA-NAG8 complex [45].

Different conformations of NAG were captured at −1 subsite in our complexes. NAG6 bound at subsite −1 (Fig. 1**B and 4C**) mimics the characteristic boat conformation that occurs in the previous step to the formation of the catalytic oxazolinium intermediate. This represents the enzyme-substrate productive complex. In contrast, both NAG4 complexes show a thermodynamically stable chair configuration at the subsite −1 that mimics the reaction product from a longer substrate (Fig. 1**C, 1D and 4E**). A distorted sugar conformation at subsite −1 is a common requirement in GH enzymes for the hydrolysis. As it was reported first for SmChiA [45], this distortion is mediated by a change in the polar link pattern among the carboxylates within the DXDXE motif. Our Asp169/Glu171 double mutation precludes observation of this issue, but it is reflected in the double conformation of the middle Asp169 observed in the unbound enzyme [20]. In all complexes, the NAG positioned at subsite −1 is stacked to the conserved Trp378 [33]. In addition, Asp240 and Tyr293 make direct polar link to O6, while Trp131 NH main-chain is linked to O3.

The main difference between the substrate and the product is the free hydroxyl of NAG4, which is close to Met237 and Tyr239. These are highly conserved along the GH18, Tyr239 making hydrogen link to the NAG4 hydroxyl. This means that one extra hydrogen bond and an extra interaction contribute to the stabilization of the reaction products**.** It should be noted that in this subsite, the presence of three cis peptides (Phe71, Glu171, W378), preserves the peptide geometry for ligand binding [34].

### *3.5. The distinct substrate/product binding modes at the aglycone and the dynamic mechanism*

Despite the sole presence of NAG4 in the solution of the cocrystallization and soaked crystals, a clear electron density map reveals only a NAG2 moiety in the reducing end subsites of both complexes. A possible explanation is the lack of further subsites, which makes a looser binding with the resulting disorder. Also, the presence of NAG2 as a contaminant or as a product of residual catalytic activity cannot be discarded. As said, the NAG unit of the NAG2 molecule located in the subsite +1 of the Chit42-NAG4/NAG2 cocrystallization complex is displaced to that observed in the NAG6 complex (see Fig. 4**A**). This may be related to the shift observed at the CID domain upon Chit42-NAG6 complex formation (Fig. 2**B and 2C).** Thus, the CID comes closer to the sugar in the substrate complex prior to the hydrolysis, and the mobility of this domain might be important for products release. In this sense, soaking of the crystals into NAG4 may represent a previous state in which the NAG conformation at −1 has changed from the energetically unfavourable NAG6 boat form to the favourable chair form of NAG4, with the associated breakage of the covalent link, but before NAG2 migrates to the product position observed in the NAG4 cocrystallization complex. Therefore, the next paragraphs will be concentrated in the comparison between the NAG4/NAG2 by cocrystallization and the NAG6 complexes, to highlight the different substrate/product binding mode.

Subsite +1 is defined by Trp131, which has a poorly defined density in the wild type indicating some flexibility, but that is well ordered upon complex formation, indicating that this Trp serves as a subsite +1 platform **(**Fig. 4**D and 4F)**. The capability of the aromatic ring to flip is important for the formation and maintenance of the substrate binding sites, performing a productive sliding of the substrate and required for the −1 distortion, as was reported in AfChiB1 [33]. Moreover, the CID residue Arg295 is conserved, having a relevant role removing sugars from the reducing end. It interacts with the NAG CO in both, the substrate and the product, and its role may be crucial in the releasing event due to its side chain flexibility that can accompany the NAG upon product release.

Major differences in the interaction pattern are observed in this position, as a large shift of the NAG occupying the +1 subsite is detected in the product NAG2 complex (Fig. 4**D and 4F**). Consequently, the direct hydrogen link between the sugar O6 to the Tyr172 hydroxyl observed in the NAG6 substrate complex (Fig. 4**D)** is lost, but a new hydrogen bond from this O6 to Asp240 carboxylate is created in the product NAG2 (Fig. 4**F**). Furthermore, Arg295 makes an additional hydrogen link to O3 of the NAG2 product.

At +2 subsite, Asn218 coordinates an ordered water molecule that connects to the CO from NAG, while Phe245 forms a platform stacking the sugar. This Phe is conserved in AfChiB1 and SmChiA, while is a Trp in other homologues proteins as CiX1, Crchi1 or SmChiB. In addition, Tyr172 makes a direct hydrogen bond to O3 in the NAG6 complex **(**Fig. 4**D),** while the bond is mediated by a water molecule in the complex with the product NAG2 **(**Fig. 4**F)**. The tilt of Tyr172 in both complexes indicates that flexibility of this residues may also contribute to substrate/product mobility. This residue is conserved in the homologues but is a Phe in SmChitA.

Consequently, while the NAG unit bound at subsite +1 is clamped to Tyr172, at the core domain, and also to Arg295 from the CID domain in the substrate NAG6, a tilt in Tyr172 releases the sugar leaving the product NAG2 associated mostly to the CID domain, which subsequently retracts by >2 Å and withdraws the product (Fig. 5**A).** Thus, the movement of the loop 243–250 (β6-α6) including the Phe245 is coupled with the shift observed at the CID domain. As it is shown in the figure, there is a net of hydrogen bonds close to subsites −1 and +1 that tether one edge of the CID to the catalytic domain, allowing the opposite edge to swing, and a series of mostly hydrophobic residues move apart in a concerted way with Phe245, which places the ring at subsite +2. Interestingly, the flexibility of the Chit42 CID domain and its concerted movement with the loop β6-α6 is evidenced and well depicted by the ensemble refinement procedure performed with the native

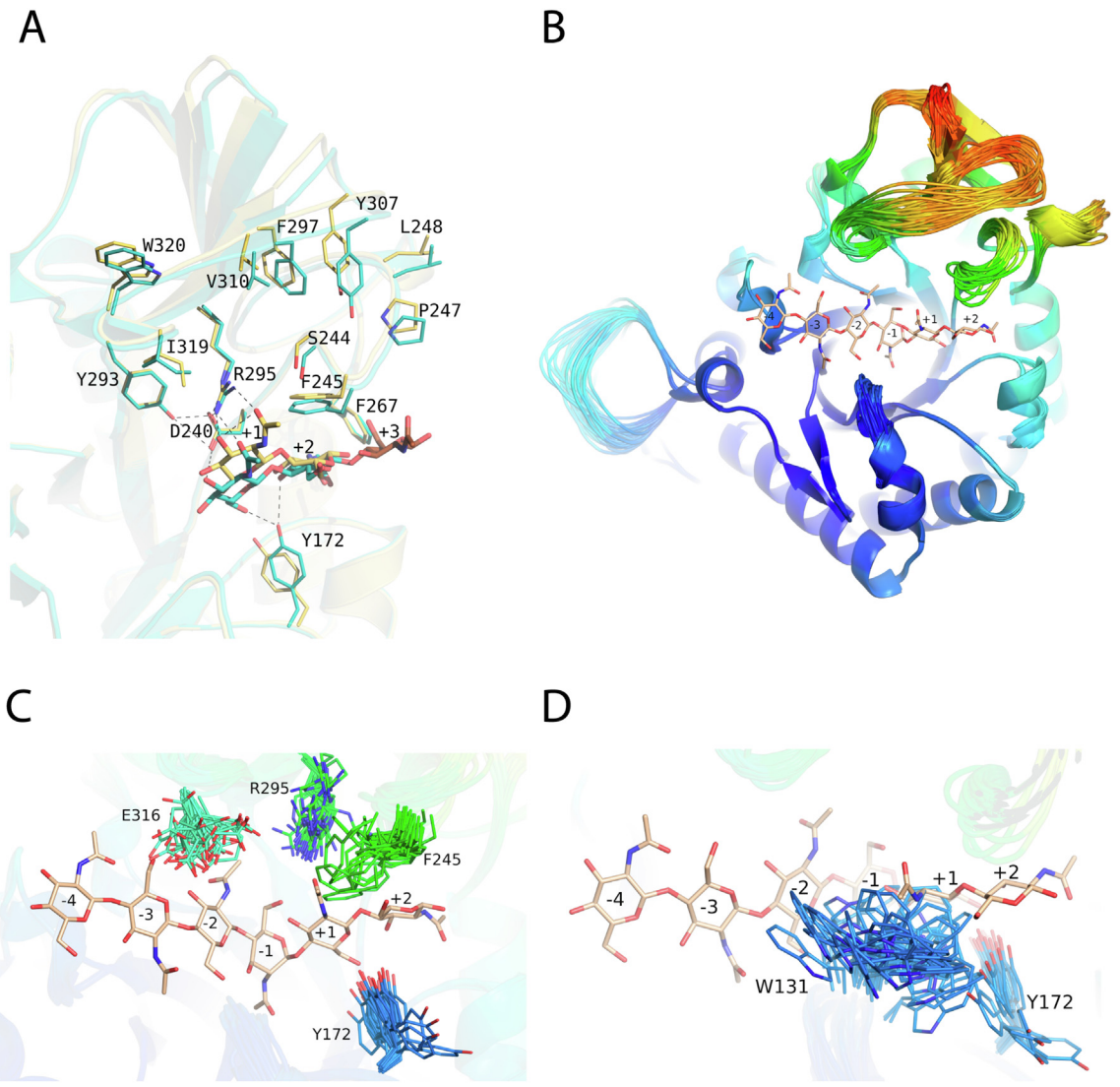


**Fig. 5. Chit42 dynamic mechanism**. A) Structural changes observed in the *positive* subsites upon substrate (cyan) or product (yellow) binding, highlighting that the NAG2 product remains linked only to the CID domain. A subsequent NAG unit (brown sticks) would not present atomic interactions with the enzyme. The putative position of this NAG moiety has been extrapolated from superimposition of the complex SmChiB-NAG5 (PDB code 1E6N) onto Chit42-NAG6. B) Ensemble refinement performed with the native Chit42 coordinates showing potential conformers of the polypeptide chain (color code gives chain mobility, from low in blue to high in red). NAG6 from the complex is shown as sticks. C) and D) Zoom of panel B highlighting the generated ensemble models of relevant residues as sticks. (For interpretation of the references to color in this figure legend, the reader is referred to the web version of this article.)

coordinates (Fig. 5**B**), which gives dynamic details of the protein by combining X-ray structure refinement with molecular dynamics. Moreover, a close inspection to the generated ensemble models highlights the flexibility of the Phe245, Arg295, Glu316 side-chains and shows their different conformations that may guide the substrate entrance and the products release along the different steps of the reaction described above (Fig. 5**C**). Furthermore, and most remarkably, despite Tyr172 being located in a well-ordered loop, its side-chain undergoes very large displacements that are consistent with its role as a switch swapping the substrate/product bound states. Moreover, as it is observed in Fig. 5**D,** changes in this Tyr172 side-chain appear coupled to the dynamic Trp131 position, and therefore both movements could be associated to the progress of the catalytic reaction. Consequently, the mobility observed in of theses residues might provide additional mechanisms cooperating with the aromatics to ensure processivity of Chit42.

Remarkably, a lower sequence conservation at this subsite +2 shapes different cavities, leading to large differences among homologues. In particular, the CID region between β7a-β7b, which shapes the upper wall of the tunnel at the positive subsites, has low sequence identity, with longer loops in SmChiA and human hcgp-39 (**Figure S1**). Therefore, subtle molecular mechanisms may operate modulating different specificities and, consequently, different transglycosilation efficacy. On the other hand, the analysis of the Chit42 active site suggests that there are no additional binding sites further to +2 subsite, as a subsequent NAG unit would not present significant atomic interactions with the enzyme (Fig. 5). This issue is relevant to consider potential acceptor substrates for biosynthetic transglycosylation reaction.

### *3.6. Role of relevant residues by mutagenesis and engineering of improved activities*

We have explored the role of the residues showing large conformational changes in our different complexes and the ensemble refinement and therefore with a potential role in binding and activity. Thus, mutation on Glu316, making many polar interactions at subsites −3 and −2, and on Tyr172, Phe245 and Arg295, being

involved in the structural changes observed at the positive moiety including the CID domain, were analysed to correlate these observations with the function. Table 1 shows the hydrolytic activity of the Chit42 variants on several substrates differing in size and DD. Except for the R295S substitution, and slightly for E316N, all the mutations reduce, a priori, the protein specific activity on colloidal chitin, albeit to varying extents. This effect is larger when they were tested on the short, acetylated substrate NAG6, although the variants R295S and E316S were only slightly affected. In contrast, none of the substitutions reduced the activity of the protein on chitosan CHIT50 (77% DD), with variants R295A and E316A having two-fold, R295S three-fold, and E316S five-fold activity, as compared to the wild-type. Finally, a similar effect on the almost deacetylated CHIT100 is observed, with a notable 40-fold increment of activity in the R295S mutant. Consequently, changes on these positions seem to impair activity mostly in the acetylated substrates, while activity on chitosan is not affected or even enhanced.

To further explore the putative role of these positions in activity, kinetic analyses of all the protein variants were carried out on colloidal chitin (Table 2) and NAG6 (Table 3) and supplementary **Figure S4**. The high viscosity developed by the corresponding solutions on increasing substrate concentration prevented the kinetic assays of the two chitosans. As seen in Table 2, most variants show a decreased substrate affinity, with 2–3 fold incremented $K_m$ values, and up to 10-fold lower $k_{cat}$ leading to notably less efficient enzymes on chitin. Two exceptions are R295S, with a four-fold superior $k_{cat}$, and E316S, with a seven-fold decreased $K_m$, both leading to slightly enhanced enzymes. A similar decreased catalytic efficiency of Chit42 was obtained in the variants by using NAG6 as substrate, with the exceptions of the above mentioned R295S and E316S, which show catalytic efficiency improved by two and four, respectively (Table 3). Therefore, these results ascribe a relevant role to these positions in the chitinolytic activity of Chit42.

The activity trends observed upon the different Chit42 changes may be elucidated on the basis of our structural results. First of all, Tyr172 is a residue conserved in fungal, plants and human enzymes (but a Phe in SmChiA) located in the short β4-α4 loop after the DXDWE motif. The analysis of our complexes showed that it makes two direct hydrogen bonds to the substrate NAG6 in subsites +1 and +2 but none to the product NAG4, supporting a role in the structural changes that facilitate product release. Accordingly, its replacement to Glu or Phe drops the specific activity on chitin and NAG6, but no effect is evident on chitosan (Table 1). The removal of the Tyr side-chain should prevent the formation of the two polar links to the substrate with an associated decreased in its substrate affinity to subsites +1 and +2. Following Kurasin *et al* [46] this would result in a diminished "pushing potential". A high "pushing potential" (high binding affinity to +1 +2 subsites) together with low "off-rates" (high binding affinity to −2 and −1 subsites) are proposed as key factor determining processive action of GH18 enzymes [46] Therefore, the Y172F and Y172E changes may weak the sliding ability of Chit42, which seems to affect principally the activity on polymeric/oligomeric acetylated substrates as chitin and NAG6, even when Tyr172 is not making any link to the N-acetyl moiety. This agrees with the increased $K_m$ and decreased $k_{cat}$ resulting in very inefficient enzymes vs chitin and NAG6, as shown in Tables 2 and 3. Previously, a complete inactivation of SmChiB was reported by removal of the equivalent Tyr (Y145A mutant), which was attributed by theoretical simulation to a stabilization role of Tyr on the strand including the catalytic motif [16]**.** On the contrary, the opposite effect was observed upon the Y160A mutant on SpChiD (Y154A numbering in the PDB coordinates), with an increase in the hydrolytic activity while retaining the innate transglycosilating activity of the enzyme [47]**.** Despite both enzymes having common non-reducing hydrolytic activity, this disparate effect caused by the Y/A change suggests different putative roles even when considering conserved residues. Moreover, the high flexibility of Tyr172 suggested by the ensemble refinement of Chi42 would not be possible in the two bacterial enzymes, as the equivalent Tyr is occluded by the bulk Phe191 and Trp160 in SmChiB and SpChiD, respectively (**Figure S5A** in supplementary material). Therefore, the postulated role of Tyr172 as a switch swapping the substrate/product bound states might possibly be a trait particular to fungal enzymes.

Arg295 is a conserved residue in fungal and bacteria enzymes but is substituted by Tyr in plants. It is located at the first β-strand of the CID domain, participating in a hydrogen bonding network to Asp240 and Tyr293 that links the CID domain to the loop β6-α6 (Fig. 5). This polar network functions as a hinge pivoting the shift of the CID domain observed in our complexes. Arg295 is also involved in making a polar link to the CO from the N-acetyl moiety of NAG bound at subsite +1. In the complex with NAG4, and after losing the link with Tyr172, the product approximates to Arg295 and makes two additional links through O3 and O6 atoms. Thus, after the cleavage of the glycoside bond, Arg295 may assist in drawing the product away from the catalytic site, which would contribute to the proposed pushing potential promoting processivity. In agreement with this, its change to Ala or Thr is deleterious for activity on chitin and NAG6 (when is evaluable), which is a consequence of, both, apparent decreased substrate affinity and $k_{cat}$ value (Table 2 and 3). Again, and as said above, the activity on almost deacetylated chitosan is not apparently affected in these variants. Previously, removal of the Arg side-chain was reported to keep the hydrolytic activity of the SmChiB R294A mutant on crystalline β-chitin [16]**,** while decreased hydrolytic but increased transglycosilating activity on NAG4 was reported on the R284A

**Table 1**
Activity of the Chit42 variants on different substrates.

| | Colloidal Chitin | NAG6 | CHIT50 | CHIT100 |
|---|---|---|---|---|
| WT | 1.4 ± 0.03 | 3.80 ± 0.2 | 0.8 ± 0.03 | 0.1 ± 0.02 |
| Y172E | 0.8 ± 0.04 | 0.30 ± 0.02 | 1.0 ± 0.04 | 0.1 ± 0.01 |
| Y172F | 0.7 ± 0.02 | 0.12 ± 0.06 | 1.0 ± 0.03 | 0.2 ± 0.02 |
| F245N | 0.9 ± 0.06 | 0.30 ± 0.01 | 1.1 ± 0.05 | n.a |
| R295A | 0.5 ± 0.02 | 0.29 ± 003 | 1.6 ± 0.06 | 0.1 ± 0.01 |
| R295S | 6.8 ± 0.05 | 2.93 ± 0.06 | 2.4 ± 0.03 | 4.4 ± 0.2 |
| R295T | 0.6 ± 0.03 | 0.14 ± 0.01 | 1.0 ± 0.01 | 0.04 ± 0.01 |
| E316A | 1.1 ± 0.01 | 0.20 ± 0.01 | 1.6 ± 0.05 | 0.6 ± 0.05 |
| E316N | 1.8 ± 0.15 | 0.23 ± 0.04 | 1.4 ± 0.04 | 0.3 ± 0.02 |
| E316S | 0.9 ± 0.08 | 3.10 ± 0.06 | 4.2 ± 0.6 | n.a |

Specific activity data (U $mg^{-1}$ of protein) are average of 3 independent experiments and standard errors are indicated. Colloidal chitin, chitosan CHIT50 and chitosan CHIT100, all 8 mg $mL^{-1}$, NAG6 300 μM.
n.a.: no activity evaluated.

**Table 2**
Catalytic functions of the Chit42 variants on colloidal chitin.

| | $K_m$ (mg mL$^{-1}$) | $V_{max}$ (μmol min$^{-1}$) | $k_{cat}$ (s$^{-1}$) | $k_{cat}/K_m$ (s$^{-1}$ mL mg$^{-1}$) |
|---|---|---|---|---|
| WT | 4.7 ± 1.1 | 0.11 ± 0.01 | 60.1 ± 6 | 12.8 ± 3 |
| Y172E | >5 | >0.08 | >16 | n.e |
| Y172F | 9.6 ± 0.9 | 0.26 ± 0.01 | 5.9 ± 0.3 | 0.6 ± 0.06 |
| F245N | 7.7 ± 1.3 | 0.14 ± 0.01 | 23 ± 2.2 | 3.1 ± 0.5 |
| R295A | >5 | >0.04 | >8.2 | n.e |
| R295S | 13.6 ± 0.9 | 0.11 ± 005 | 260 ± 13 | 19.5 ± 1.3 |
| R295T | 13.1 ± 3.6 | 0.20 ± 0.03 | 21 ± 3.4 | 1.6 ± 0.4 |
| E316A | 10.2 ± 1.5 | 0.37 ± 0.03 | 36.8 ± 3.7 | 3.6 ± 0.4 |
| E316N | 9.9 ± 1.1 | 0.36 ± 0.02 | 58.8 ± 3.6 | 5.9 ± 0.6 |
| E316S | 0.7 ± 0.2 | 0.006 ± 0.0005 | 14.9 ± 1.2 | 19.8 ± 6 |

Reaction velocity measurements were performed in triplicate and standard errors are indicated. n.e., not evaluable. $K_{cat}$ calculated from $V_{max}$ determinations considering 42 kDa for Chit42.

**Table 3**
Catalytic functions of the Chit42 variants on NAG6.

| | $K_m$ (μM) | $V_{max}$ (μmol min$^{-1}$) | $k_{cat}$ (s$^{-1}$) | $k_{cat}/K_m$ (s$^{-1}$ μM$^{-1}$) |
|---|---|---|---|---|
| WT | 641 ± 106 | 0.69 ± 0.06 | 376 ± 38 | 0.59 ± 0.09 |
| Y172E | 1320 ± 700 | 0.15 ± 0.06 | 30 ± 12 | 0.02 ± 0.012 |
| Y172F | 685 ± 300 | 0.08 ± 0.02 | 6.7 ± 1.6 | 0.009 ± 0.003 |
| F245N | 1215 ± 600 | 0.23 ± 0.06 | 37 ± 10 | 0.03 ± 0.01 |
| R295A | >500 | >0.125 | >25.7 | n.e |
| R295S | 476 ± 240 | 0.05 ± 0.01 | 962 ± 20 | 1.3 ± 0.6 |
| R295T | 882 ± 350 | 0.11 ± 0.02 | 11 ± 3 | 0.012 ± 0.005 |
| E316A | >500 | >0.1 | >10 | n.e. |
| E316N | 1133 ± 420 | 0.11 ± 0.02 | 17 ± 4 | 0.015 ± 0.005 |
| E316S | 1108 ± 630 | 0.10 ± 0.04 | 2815 ± 1098 | 2.5 ± 1.4 |

Reaction velocity measurements were performed in triplicate and standard errors are indicated. n.e., not evaluable. $k_{cat}$ calculated from $V_{max}$ determinations considering 42 kDa for Chit42.

mutant (R278 in the PDB coordinates) of SpChiD [47]**.** The decreased activity observed on colloidal chitin and NAG6 is consistent with that observed in the SmChiD mutant**.** Supplementary Figure S5B shows that the network of the polar links established by Arg295 and its role in binding the subtrate in subsite +1 is shared with the two bacterial enzymes. However, the large structural differences of the β7α-β7β loop within the corresponding CID domains may explain the different results obtained upon removal of the Arg side-chain. Furthermore, the increased activity observed upon the R295S replacement on all the substrates is difficult to explain. It might be that the mutation produces a rearrangement of the polar interactions network among Tyr293, Asp240 and Arg295, linking the catalytic and the CID domains, with a resulting change in the mobility of the CID domain that improve products release events (Supplementary **Figure S6**). This agrees with the marked increase in the $k_{cat}$ calculated for the chitin and NAG6 hydrolysis by the R295S change as given in Table 2 and 3, which may result in an enzyme somewhat more catalytic efficient than the native enzyme.

Phe245, either Phe or Trp in homologues, is located at loop β6-α6, which shows structural changes coupled to the CID domain upon substrate binding (Fig. 5). It defines subsite +2 by stacking to bound NAG and, therefore, the general decreased activity of the F245N variant shown in Tables 1, 2 and 3 could be expected, although a slightly increased specific activity on chitosan CHIT50 is apparent. Previous results reported that the mutation F396A, the equivalent residue in SmChitA, had little impact on hydrolysis of crystalline chitin and only moderate impact on processive ability on chitosan [15], which was explained as this Phe having little role in ligand binding by calculating the free energy through experimental and MD simulation techniques [42]. However, the replacement of Phe by Trp increases markedly its transglycosilation ability [18] revealing a role in acceptor substrate binding. Nevertheless, it is worth noting that, while loop β6-α6 of the SmChitA is quite conserved with Chit42, the adjacent CID domain is the most variable region and, in particular, SmChitA presents longer β7aβ7b and β7b-β7c loops (**Figure S1**). Consequently, different molecular mechanism may operate in the bacterial SmChitA. Our results show decreased affinity and $k_{cat}$ value, resulting in a less efficient F245 variant hydrolyzing colloidal chitin and NAG6 (Table 2 and 3). The effect of this change in the transfructosylating ability of Chit42 remains to be investigated.

Glu316, located before β7β of the CID domain, is a conserved residue in fungal, and human homologues but not in plants nor in bacteria (supplementary **Figure S2**). It protrudes at the negative part of the active site making polar links to NAG O6 and O3 atoms bound at the subsites −3 and −2, and also to the N-acetyl moiety at subsite −2, which could stabilize substrate binding possibly decreasing "off-rates" and promoting processivity. Accordingly, a general reduction of the specific activity on chitin and NAG6 is detected upon its change, but an improvement on chitosan similarly to that obtained by the changes R295S/A is observed (Table 1). This position is a Glu in SmChiA, but has no equivalent in SmChiB, nor SpChiD both presenting a very different active site at this negative moiety (supplementary **Figure S5C**), which is their product binding site. An intriguing case is the E316S variant, which presents a five-fold increased activity on CHIT50, while no activity on CHIT100 was evaluated in our assay conditions. Moreover, the kinetic experiments revealed that this variant is apparently more efficient than the wild-type enzyme on chitin and NAG6, but based on a lower $K_m$ or an increased $k_{cat}$, respectively (Table 2 and 3). Therefore, the E316S variant could be a potential candidate for degrading chitin and partially deacetylated chitosan, although it is difficult to find the rationale behind this behaviour.

It has been reported that while processivity is essential for efficient degradation of crystalline chitin, it reduces the catalytic efficiency toward more soluble substrates with higher diffusion rates. This is explained in terms of the different rate-limiting steps of the

hydrolysis of soluble and insoluble substrates, processivity being at a cost in terms of intrinsic enzyme speed [15]. Thus, removal of aromatics near the catalytic site led to impaired activity of bacterial chitinases on crystalline chitin while moderate or even high efficiency was observed on chitosan. A similar trend has been observed in our work upon changes in residues associated to the CID domain movement. This might suggest that the dynamic structural changes described in Chit42 might represent a supplementary mechanism contributing to its processive ability, at least in the fungal homologues. It is worth noting that GH18 processive enzyme share many structural features as the insertion domain and the aromatics, but these properties are not ensuring processivity [9]. Moreover, only a few studies report the contribution of polar residues in substrate binding and processivity [16]. Therefore, a full understanding of the molecular mechanisms of processivity remains elusive.

Finally, it should be noted that R295 and E316 are residues linking the N-acetyl moiety at +1 and −2 subsites and, consequently, its removal decreases the Chit42 activity on chitin and NAG6, while not affecting or even enhancing activity on deacetylate chitosan. In particular, the R295S variant is an interesting enzyme with improved activity on all substrates, while E316S and E316A could be good targets to be used for more efficient hydrolysis of CHIT50 and CHIT100, respectively.

## 4. Conclusions

Chitinases, as a very diverse group of enzymes, present different molecular structure, substrate specificity, and catalytic mechanism. Therefore, analysis of their substrate specificity could not only reveal their physiological roles, but is also necessary to perform an efficient bioconversion of chitin into novel products for industrial applications. Much work has been reported on the catalytic mechanism of bacterial GH18 chitinases, which revealed its substrate-assisted catalytic mechanism and the dynamic hallmarks of processivity contributing to the degradation of the crystalline polymer. Moreover, recent work has been addressed to understand structural features behind transglycosylation with the goal of making a controlled synthesis of COS. However, structural studies on fungal chitinases have focussed on their interaction with inhibitors [32–34] and only mutation on the catalytic residues have been explored to modulated their hydrolase/transferase activity [19]. We report here a detailed picture of the molecular events behind substrate/products binding in fungal Chit42, giving full insight into its donor and acceptor subsites. The crystallographic analysis of three complexes with small-chain chitooligosacharides revealed a previously unobserved dynamic on–off ligand binding process associated with motion of its CID domain accompanying the substrate towards, and the products out from, the active site. This might represent a molecular mechanism complementary to the role ascribed to the aromatics located near the catalytic site in processivity. This movement is concerted with large changes in the Tyr172 side-chain that acts as a switch swapping the substrate/product bound states. The generated ensemble models also suggest that Tyr172 may assist the role of Trp131, defining the +1 subsite, ensuring a productive slide of the substrate. The key residues linking the chitooligosaccharides and affected by this motion have been mutated, and their role in hydrolysis of chitin, chitosan and NAG6 investigated. All the changes affect the Chit42 hydrolytic activity therefore confirming the involvement of these positions in catalysis. Moreover, the fact that changes in residues associated to this CID domain movement result in unaffected or even enhanced activity vs chitosan is consistent with the negative correlation between processivity and enzyme efficiency toward soluble substrates observed before in bacterial chitinases. More intriguing is the deleterious effect observed on the hydrolysis of the soluble NAG6, which suggest that more subtle mechanisms may operate in processivity and preference/tolerance for acetylated/deacetylated sugars.

Further work is ongoing to explore the hydrolytic activity and product specificity of the promising mutants to fine-tune Chit42 activity. This will facilitate the design and mutation strategies to develop chitinases with enhanced antifungal, hydrolytic or transglycosilating properties.

## 5. Accession number

The coordinates and structure factors of Chit42 complexed with NAG6, NAG4/NAG2

(cocrystallization) and NAG4/NAG2 (soaking) have been deposited in the Protein Data Bank with the accession codes 6YLJ, 6YN4 and 7AKQ.

## CRediT authorship contribution statement

**Elena Jiménez-Ortega:** Investigation, Methodology, Formal analysis, Writing – original draft, Writing – review & editing. **Peter Elias Kidibule:** Investigation, Formal analysis, Methodology. **María Fernández-Lobato:** Conceptualization, Formal analysis, Funding acquisition, Writing – review & editing. **Julia Sanz-Aparicio:** Conceptualization, Formal analysis, Funding acquisition, Methodology, Writing – original draft, Writing – review & editing.

## Declaration of Competing Interest

The authors declare that they have no known competing financial interests or personal relationships that could have appeared to influence the work reported in this paper.

## Acknowledgements

This work was supported by grants from the Spanish Ministry of Economy and Competitiveness through grants BIO2016-76601-C3-3-R/-C3-2-R, PID2019-105838RB-C33/-C32, Fundación Ramón Areces [XIX Call of Research Grants in Life and Material Sciences] and EU EMFF-Blue Economy-2018 [Fish4Fish-863697]. We are grateful to the staff of the Synchrotron Radiation Sources at Alba (Barcelona, Spain) for providing access and for technical assistance at BL13-XALOC beamline and to the Fundación Ramón Areces for an institutional grant to the Centre of Molecular Biology Severo Ochoa.

## Appendix A. Supplementary data

Supplementary data to this article can be found online at https://doi.org/10.1016/j.csbj.2021.09.027.

## References

[1] Qu T, Zhang C, Qin Z, Fan L, Jiang L, Zhao L. A novel GH Family 20 β-N-acetylhexosaminidase with both chitosanase and chitinase activity from *Aspergillus oryzae*. Front Mol Biosci 2021;8:1–10. https://doi.org/10.3389/fmolb.2021.684086.

[2] Rinaudo M. Chitin and chitosan: Properties and applications. Progress in Polymer Science (Oxford) 2006;31(7):603–32. https://doi.org/10.1016/j.progpolymsci.2006.06.001.

[3] Rathore AS, Gupta RD. Chitinases from bacteria to human: Properties, applications, and future perspectives. Enzyme Research 2015;2015:1–9. https://doi.org/10.1155/2015/791907.

[4] Hamed I, Özogul F, Regenstein JM. Industrial applications of crustacean by-products (chitin, chitosan, and chitooligosaccharides): A review. Trends Food Sci Technol 2016;48:40–50. https://doi.org/10.1016/j.tifs.2015.11.007.

[5] Tabassum N, Ahmed S, Ali MA. Chitooligosaccharides and their structural-functional effect on hydrogels: A review. Carbohydr Polym 2021;261:117882. https://doi.org/10.1016/j.carbpol.2021.117882.
[6] Heggset EB, Dybvik AI, Hoell IA, Norberg AL, Sørlie M, Eijsink VGH, et al. Degradation of chitosans with a family 46 chitosanase from *Streptomyces coelicolor* A3(2). Biomacromolecules 2010;11(9):2487–97. https://doi.org/10.1021/bm1006745.
[7] Synstad B, Gaseidnes S, van Aalten DMF, Vriend G, Nielsen JE, Eijsink VGH. Mutational and computational analysis of the role of conserved residues in the active site of a family 18 chitinase. Eur J Biochem 2004;271(2):253–62. https://doi.org/10.1046/j.1432-1033.2003.03923.x.
[8] van Aalten DMF, Komander D, Synstad B, Gaseidnes S, Peter MG, Eijsink VGH. Structural insights into the catalytic mechanism of a family 18 exo-chitinase. Proc Natl Acad Sci 2001;98(16):8979–84. https://doi.org/10.1073/pnas.151103798.
[9] Chen W, Jiang Xi, Yang Q. Glycoside hydrolase family 18 chitinases: The known and the unknown. Biotechnol Adv 2020;43:107553. https://doi.org/10.1016/j.biotechadv.2020.107553.
[10] Horn SJ, Sorbotten A, Synstad B, Sikorski P, Sorlie M, Varum KM, et al. Endo/exo mechanism and processivity of family 18 chitinases produced by *Serratia marcescens*. FEBS J 2006;273(3):491–503. https://doi.org/10.1111/ejb.2006.273.issue-310.1111/j.1742-4658.2005.05079.x.
[11] Eijsink VGH, Vaaje-Kolstad G, Vårum KM, Horn SJ. Towards new enzymes for biofuels: lessons from chitinase research. Trends Biotechnol 2008;26(5):228–35. https://doi.org/10.1016/j.tibtech.2008.02.004.
[12] Sørlie M, Horn SJ, Vaaje-Kolstad G, Eijsink VGH. Using chitosan to understand chitinases and the role of processivity in the degradation of recalcitrant polysaccharides. React Funct Polym 2020;148:104488. https://doi.org/10.1016/j.reactfunctpolym.2020.104488.
[13] Horn SJ, Sikorski P, Cederkvist JB, Vaaje-Kolstad G, Sørlie M, Synstad B, et al. Cost and benefits of processivity in enzymatic degradation of recalcitrant polysaccharides. PNAS 2006;103:18089–94. https://doi.org/10.1073/pnas.0608909103.
[14] Vaaje-Kolstad G, Horn SJ, Sørlie M, Eijsink VGH. The chitinolytic machinery of Serratia marcescens - A model system for enzymatic degradation of recalcitrant polysaccharides. FEBS J 2013;280:3028–49. https://doi.org/10.1111/febs.12181.
[15] Zakariassen H, Aam BB, Horn SJ, Vårum KM, Sørlie M, Eijsink VGH. Aromatic residues in the catalytic center of chitinase A from *Serratia marcescens* affect processivity, enzyme activity, and biomass converting efficiency. J Biol Chem 2009;284(16):10610–7. https://doi.org/10.1074/jbc.M900092200.
[16] Jana S, Hamre AG, Eijsink VGH, Sørlie M, Payne CM. Polar residues lining the binding cleft of a *Serratia marcescens* family 18 chitinase position the substrate for attack and stabilize associative interactions. Mol Phys 2019;117(23–24):3664–82. https://doi.org/10.1080/00268976.2019.1657600.
[17] Zakariassen H, Hansen MC, Jøranli M, Eijsink VGH, Sørlie M. Mutational effects on transglycosylating activity of family 18 chitinases and construction of a hypertransglycosylating mutant. Biochemistry 2011;50(25):5693–703. https://doi.org/10.1021/bi2002532.
[18] Madhuprakash J, Dalhus B, Rani TS, Podile AR, Eijsink VGH, Sørlie M. Key residues affecting transglycosylation activity in family 18 chitinases: Insights into donor and acceptor subsites. Biochemistry 2018;57(29):4325–37. https://doi.org/10.1021/acs.biochem.8b00381.
[19] Martinez EA, Boer H, Koivula A, Samain E, Driguez H, Armand S, et al. Engineering chitinases for the synthesis of chitin oligosaccharides: Catalytic amino acid mutations convert the GH-18 family glycoside hydrolases into transglycosylases. J Mol Catal B Enzym 2012;74(1-2):89–96. https://doi.org/10.1016/j.molcatb.2011.09.003.
[20] Kidibule PE, Santos-Moriano P, Jiménez-Ortega E, Ramírez-Escudero M, Limón MC, Remacha M, et al. Use of chitin and chitosan to produce new chitooligosaccharides by chitinase Chit42: Enzymatic activity and structural basis of protein specificity. Microb Cell Fact 2018;17(1). https://doi.org/10.1186/s12934-018-0895-x.
[21] Kidibule PE, Costa J, Atrei A, Plou FJ, Fernandez-Lobato M, Pogni R. Production and characterization of chitooligosaccharides by the fungal chitinase Chit42 immobilized on magnetic nanoparticles and chitosan beads: selectivity, specificity and improved operational utility. RSC Adv 2021;11(10):5529–36. https://doi.org/10.1039/D0RA10409D.
[22] Álvaro-Benito M, de Abreu M, Portillo F, Sanz-Aparicio J, Fernández-Lobato María. New insights into the fructosyltransferase activity of *Schwanniomyces occidentalis* β-fructofuranosidase, emerging from nonconventional codon usage and directed mutation. Appl Environ Microbiol 2010;76(22):7491–9. https://doi.org/10.1128/AEM.01614-10.
[23] Kabsch W. XDS. Acta Crystallogr D Biol Crystallogr 2010;66(2):125–32. https://doi.org/10.1107/S0907444909047337.
[24] Evans PR, Murshudov GN. How good are my data and what is the resolution? Acta Crystallogr D Biol Crystallogr 2013;69(7):1204–14. https://doi.org/10.1107/S0907444913000061.
[25] Winn MD, Ballard CC, Cowtan KD, Dodson EJ, Emsley P, Evans PR, et al. Overview of the CCP4 suite and current developments. Acta Crystallogr D Biol Crystallogr 2011;67(4):235–42. https://doi.org/10.1107/S0907444910045749.
[26] Murshudov GN, Vagin AA, Dodson EJ. Refinement of macromolecular structures by the maximum-likelihood method. Acta Crystallogr D Biol Crystallogr 1997;53(3):240–55. https://doi.org/10.1107/S0907444996012255.
[27] Emsley P, Cowtan K. Coot: Model-building tools for molecular graphics. Acta Crystallogr D Biol Crystallogr 2004;60(12):2126–32. https://doi.org/10.1107/S0907444904019158.
[28] Adams PD, Afonine PV, Bunkóczi G, Chen VB, Davis IW, Echols N, et al. A comprehensive Python-based system for macromolecular structure solution. Acta Crystallogr D Biol Crystallogr 2010;66(2):213–21. https://doi.org/10.1107/S0907444909052925.
[29] Tom Burnley B, Afonine P v., Adams PD, Gros P. Modelling dynamics in protein crystal structures by ensemble refinement. ELife 2012;2012:1–29. https://doi.org/10.7554/eLife.00311.
[30] DeLano L, Pymol W. An open-source molecular graphics tool. CCP4 Newsletter On Protein Crystallography 2002;40:1–8.
[31] Li H, Greene LH, Yang H. Sequence and structural analysis of the chitinase insertion domain reveals two conserved motifs involved in chitin-binding. PLoS ONE 2010;5(1):e8654. https://doi.org/10.1371/journal.pone.0008654.
[32] Yang J, Gan Z, Lou Z, Tao N, et al. Crystal structure and mutagenesis analysis of chitinase CrChi1 from the nematophagous fungus *Clonostachys rosea* in complex with the inhibitor caffeine. Microbiology 2010;156:3566–74. https://doi.org/10.1099/mic.0.043653-0.
[33] Rao FV, Houston DR, Boot RG, Aerts JMFG, Hodkinson M, Adams DJ, et al. Specificity and affinity of natural product cyclopentapeptide inhibitors against *A. fumigatus*, human, and bacterial chitinases. Chem Biol 2005;12(1):65–76. https://doi.org/10.1016/j.chembiol.2004.10.013.
[34] Hollis T, Monzingo AF, Bortone K, Ernst S, Robertus JD, Cox R. The X-ray structure of a chitinase from the pathogenic fungus *Coccidioides immitis*. Protein Sci 2000;9(3):544–51. https://doi.org/10.1110/ps.9.3.544.
[35] Juárez-Hernández EO, Casados-Vázquez LE, Brieba LG, Torres-Larios A, Jimenez-Sandoval P, Barboza-Corona JE. The crystal structure of the chitinase ChiA74 of *Bacillus thuringiensis* has a multidomain assembly. Sci Rep 2019;9:1–10. https://doi.org/10.1038/s41598-019-39464-z.
[36] Aronson NN, Halloran BA, Alexyev MF, Amable L, Madura JD, Pasupulati L, et al. Family 18 chitinase-oligosaccharide substrate interaction: Subsite preference and anomer selectivity of *Serratia marcescens* chitinase A. Biochem J 2003;376(1):87–95. https://doi.org/10.1042/bj20030273.
[37] Fusetti F, von Moeller H, Houston D, Rozeboom HJ, Dijkstra BW, Boot RG, et al. Structure of human chitotriosidase: Implications for specific inhibitor design and function of mammalian chitinase-like lectins. J Biol Chem 2002;277(28):25537–44. https://doi.org/10.1074/jbc.M201636200.
[38] Madhuprakash J, Singh A, Kumar S, Sinha M, Kaur P, Sharma S, et al. Structure of chitinase D from *Serratia proteamaculans* reveals the structural basis of its dual action of hydrolysis and transglycosylation. International Journal of Biochemistry and Molecular Biology 2013;4:166–78.
[39] Madhuprakash J, Dalhus B, Vaaje-Kolstad G, Sakuda S, Podile AR, Eijsink VGH, et al. Structural and thermodynamic signatures of ligand binding to the enigmatic chitinase D of *Serratia proteamaculans*. J Phys Chem B 2019;123(10):2270–9. https://doi.org/10.1021/acs.jpcb.8b11448https://doi.org/10.1021/acs.jpcb.8b11448.s001.
[40] Wang Y-J, Jiang W-X, Zhang Y-S, Cao H-Y, Zhang Yi, Chen X-L, et al. Structural insight into chitin degradation and thermostability of a novel endochitinase from the glycoside hydrolase family 18. Front Microbiol 2019;10. https://doi.org/10.3389/fmicb.2019.02457.
[41] Hsieh Y-C, Wu Y-J, Chiang T-Y, Kuo C-Y, Shrestha KL, Chao C-F, et al. Crystal structures of *Bacillus cereus* NCTU2 chitinase complexes with chitooligomers reveal novel substrate binding for catalysis: A chitinase without chitin binding and insertion domains. J Biol Chem 2010;285(41):31603–15. https://doi.org/10.1074/jbc.M110.149310.
[42] Jana S, Hamre AG, Wildberger P, Holen MM, Eijsink VGH, Beckham GT, et al. Aromatic-mediated carbohydrate recognition in processive *Serratia marcescens* chitinases. J Phys Chem B 2016;120:1236–49. https://doi.org/10.1021/acs.jpcb.5b12610.
[43] Payne CM, Baban J, Horn SJ, Backe PH, Arvai AS, Dalhus B, et al. Hallmarks of processivity in glycoside hydrolases from crystallographic and computational studies of the *Serratia marcescens* chitinases. J Biol Chem 2012;287(43):36322–30. https://doi.org/10.1074/jbc.M112.402149.
[44] Houston DR, Recklies AD, Krupa JC, van Aalten DMF. Structure and ligand-induced conformational change of the 39-kDa glycoprotein from human articular chondrocytes. J Biol Chem 2003;278(32):30206–12. https://doi.org/10.1074/jbc.M303371200.
[45] Papanikolau Y, Prag G, Tavlas G, Vorgias CE, Oppenheim AB, Petratos K. High resolution structural analyses of mutant Chitinase A complexes with substrates provide new insight into the mechanism of catalysis. Biochemistry 2001;40(38):11338–43. https://doi.org/10.1021/bi010505h.
[46] Kurašin M, Kuusk S, Kuusk P, Sørlie M, Väljamäe P. Slow off-rates and strong product binding are required for processivity and efficient degradation of recalcitrant chitin by family 18 chitinases. J Biol Chem 2015;290(48):29074–85. https://doi.org/10.1074/jbc.M115.684977.
[47] Madhuprakash J, Tanneeru K, Purushotham P, Guruprasad L, Podile AR. Transglycosylation by Chitinase D from *Serratia proteamaculans* improved through altered substrate interactions. J Biol Chem 2012;287(53):44619–27. https://doi.org/10.1074/jbc.M112.400879.